NANO LETTERS

2007
Vol. 7, No. 3
766−772

Size-Dependent Magnetic Properties of Single-Crystalline Multiferroic $BiFeO_3$ Nanoparticles

Tae-Jin Park,[†] Georgia C. Papaefthymiou,[‡] Arthur J. Viescas,[‡] Arnold R. Moodenbaugh,[§] and Stanislaus S. Wong*[,†,§]

Department of Chemistry, State University of New York at Stony Brook, Stony Brook, New York 11794-3400, Department of Physics, Mendel Hall, Villanova University, 800 Lancaster Avenue, Villanova, Pennsylvania 19085, and Condensed Matter Physics and Materials Sciences Department, Brookhaven National Laboratory, Building 480, Upton, New York 11973

Received December 24, 2006

ABSTRACT

As-prepared, single-crystalline bismuth ferrite nanoparticles show strong size-dependent magnetic properties that correlate with: (a) increased suppression of the known spiral spin structure (period length of ~62 nm) with decreasing nanoparticle size and (b) uncompensated spins and strain anisotropies at the surface. Zero-field-cooled and field-cooled magnetization curves exhibit spin-glass freezing behavior due to a complex interplay between finite size effects, interparticle interactions, and a random distribution of anisotropy axes in our nanoparticle assemblies.

Multiferroics[1,2] are promising materials for the design and synthesis of multifunctional materials. They are noteworthy for their unique and strong coupling of electric, magnetic, and structural order parameters, giving rise to simultaneous ferroelectricity, ferromagnetism, and ferroelasticity.[3] In particular, ferroelectromagnets (or multiferroic magnetoelectrics) maintain a magnetization and dielectric polarization, which can be modulated and activated by an electric field and magnetic field, respectively.[4] For this reason, multiferroic materials are being considered for a host of potential applications as diverse as additives, magnetic recording media, information storage, spintronics, and sensors.[5−7]

Bismuth ferrite ($BiFeO_3$) has been a focal point of research because, in bulk form, it is an antiferromagnetic, ferroelectric, and ferroelastic multiferroic material with electrical, magnetic, and structural ordering temperatures well above room temperature. The combined action of exchange and spin−orbit interactions produces spin canting away from perfect antiferromagnetic ordering. The direction of the resulting small moment, however, rotates, superimposing a spiral spin arrangement with a wavelength of 62 nm, thereby producing a helimagnetic order and a vanishing magnetization in the bulk.[8,9] Thus far, incorporation of bismuth ferrite into practical devices has been hindered by leakage problems that lead to low resistivity, presumably due to defect and nonstoichiometry related issues. Hence, there has been a pressing need to generate high-quality samples. Recent approaches have focused on developing novel structural formulations such as zero-, one-, and two-dimensional (0-D, 1-D, and 2-D) nanostructures of $BiFeO_3$ materials.[7,10,11] The majority of prior analyses on such systems has been performed on oriented, epitaxial thin films of $BiFeO_3$ grown on a range of substrates including Si, $SrTiO_3$, $SrRuO_3$, $LaAlO_3$, $Pt/Ti/SiO_2/Si$, and $Pt/TiO_2/SiO_2/Si$.[12−16]

In spite of intense study, a fundamental understanding of structure−property correlations in $BiFeO_3$ is still lacking. Specifically, the nature of the magnetic response and the fundamental dependence of ferroelectric behavior on the size and precise chemical composition (e.g., presence of doping) are issues of deep interest.[8,17−20] Attention has recently been focused on the unique and unusual spin spiral structures of this multiferroic material.[21] However, to date, little if any effort has been expended in research associated with the synthesis of substrate-free nanostructures of $BiFeO_3$. Moreover, there have not been any viable reports on their single-crystalline nanostructure analogues associated with 0-D and/or 1-D structural motifs.

In the current work, we have employed a facile sol−gel methodology based on the glycol−gel reaction in the synthesis of single-crystalline $BiFeO_3$ nanoparticles. Their sizes have been thermodynamically controlled in order to

* To whom correspondence should be addressed. E-mail: sswong@notes.cc.sunysb.edu; sswong@bnl.gov. Telephone: 631-632-1703; 631-344-3178.
[†] State University of New York at Stony Brook.
[‡] Villanova University.
[§] Brookhaven National Laboratory.

10.1021/nl063039w CCC: $37.00
Published on Web 02/27/2007

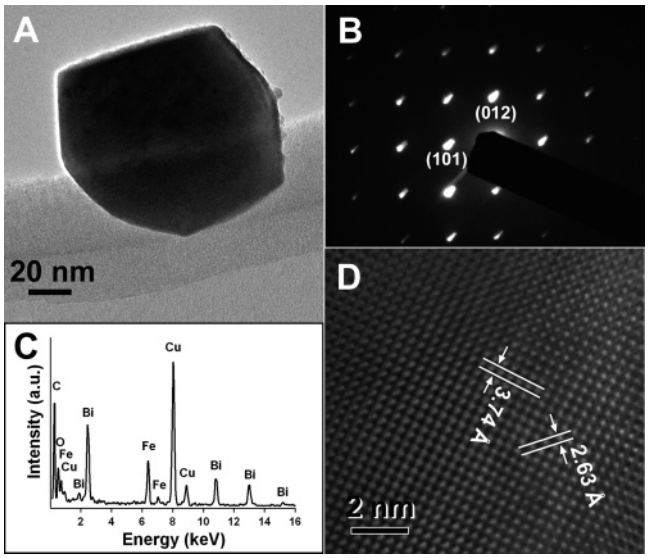

Figure 1. TEM image (A) as well as SAED pattern (B) of an individual $BiFeO_3$ nanoparticle (95 nm) generated from the annealing temperature at 600 °C and its corresponding EDS (C). The Cu and C peaks originate from the TEM grid. (D) HRTEM image of a typical portion of a corresponding $BiFeO_3$ nanoparticle.

obtain reproducible size variations ranging from less than 15 nm to greater than 100 nm. As-prepared nanoparticles of $BiFeO_3$, especially those with a diameter range on the order of or smaller than the 62 nm wavelength of their intrinsic spiral-modulated spin structure, show strong property correlations with size, an assertion which has been confirmed by superconducting quantum interference device (SQUID) and Mössbauer measurements.

Observed X-ray diffraction peak patterns of collected powders could be indexed to the rhombohedral structure of $BiFeO_3$ [space group: R_{3c}] with lattice constants of $a = b = c = 5.63$ Å and $\alpha = \beta = \gamma = 59.4°$, which are in good agreement with literature results for bulk $BiFeO_3$ (i.e., JCPDS no. 20-0169, Figure S1, Supporting Information). The sizes of our as-prepared $BiFeO_3$ nanostructures (e.g., crystalline particles with smooth faces and clear edges) annealed at 400, 450, 500, 550, 600, 650, and 700 °C were noted to be ~14 nm (uniquely obtained from XRD data using the Debye−Scherer equation), 41 ± 15 nm, 51 ± 7 nm, 75 ± 17 nm, 95 ± 28 nm, 245 ± 81 nm, and 342 ± 100 nm, respectively, as determined, from experimental scanning electron microscopy (SEM) images obtained (Figure S2, Supporting Information).

A typical transmission electron microscopy (TEM) image of as-prepared $BiFeO_3$ nanoparticles, generated at 600 °C from the current sol−gel method as described above and in the Supporting Information section, is shown in Figure 1A. Selected area electron diffraction (SAED) data taken from individual particles (Figure 1B) show the presence of sharp diffraction spots, which are indicative of the formation of well-formulated, single-crystalline $BiFeO_3$. To confirm the chemical composition of these as-prepared structures, energy dispersive X-ray spectroscopy (EDS) spectra (Figure 1C), taken at a number of selected positions of the sample, show the expected presence of Bi, Fe, and O. In Figure 1D, a high-resolution TEM image obtained from a portion of an individual $BiFeO_3$ nanoparticle is displayed in order to further confirm the single-crystalline nature of our as-prepared $BiFeO_3$ samples. This image shows a typical crystalline domain with interplanar spacings of about 3.74 and 2.63 Å, compatible with literature values for bulk $BiFeO_3$ of 3.95 and 2.81 Å, respectively (JCPDS no. 20-0169). The lattice spacings described above correspond to the {101} and {012} planes of a rhombohedral phase $BiFeO_3$ crystal. Additional TEM, HRTEM, SAED, and EDS data are shown in Figures S3 and S4 (Supporting Information).

To investigate the magnetic properties of assemblies of our bismuth ferrite nanoparticles, magnetic measurements were performed on these as well as bulk $BiFeO_3$ using a SQUID magnetometer (Figure 2). The magnetic response observed as a function of the applied magnetic field increases systematically with decreasing size of the as-prepared $BiFeO_3$ nanoparticles. Moreover, we note that the magnetic properties of bismuth ferrite nanoparticles with a mean size of 245 nm, prepared at an annealing temperature of 650 °C, show a remarkable similarity to that of the bulk. In both cases, the spontaneous magnetization measured was not appreciable.

Our SQUID results (Figure 2) suggest that a magnetic response in $BiFeO_3$ can be initiated when the size of the system is less than about 95 nm (Figure 2B). That is, whereas relatively larger $BiFeO_3$ nanoparticles, annealed at 600 °C, with an average diameter of 95 nm, display a low level of spontaneous magnetization, the magnetic response of $BiFeO_3$ nanoparticles rapidly increases in the range of 270−460% for samples below 62 nm, the period length of the spiral-modulated spin structure of $BiFeO_3$, as compared with that of the bulk. A summary of the behavior of recorded $BiFeO_3$ magnetization values as a function of size is plotted in the inset to Figure 2A. In addition, to illustrate the large hysteresis intrinsic to $BiFeO_3$ nanoparticles with dimensions smaller than 62 nm, the magnetization behavior for the smallest nanoparticles have been recorded at 10 K as well as at 300 K (Figure 2C). Magnetic parameters associated with nanoparticulate $BiFeO_3$ are summarized in Table 1. From our data (Figure 2B), it is evident that the favorable magnetic properties of $BiFeO_3$ nanoparticles with typical dimensions below 62 nm strongly correlate with the size of the nanostructures themselves due to their grain size confinement, an effect which has been found to modify the long-range spiral-modulated spin structure of $BiFeO_3$.[9,22]

An antiferromagnet can be described as comprising two spin sublattices with ferromagnetic interactions within one sublattice and antiferromagnetic interactions between sublattices. Néel[23−25] attributed the magnetic moment of small antiferromagnetic particles to incomplete magnetic compensation between these two sublattices. This incomplete spin compensation possible in antiferromagnetically ordered materials becomes measurable only in small antiferromagnetic systems, where the long-range antiferromagnetic order is frequently interrupted at the particle surfaces. In small structures, the surface-to-volume ratio becomes very large with decreasing particle size, enhancing the tangible contribution to the particle's overall magnetization by uncompen-

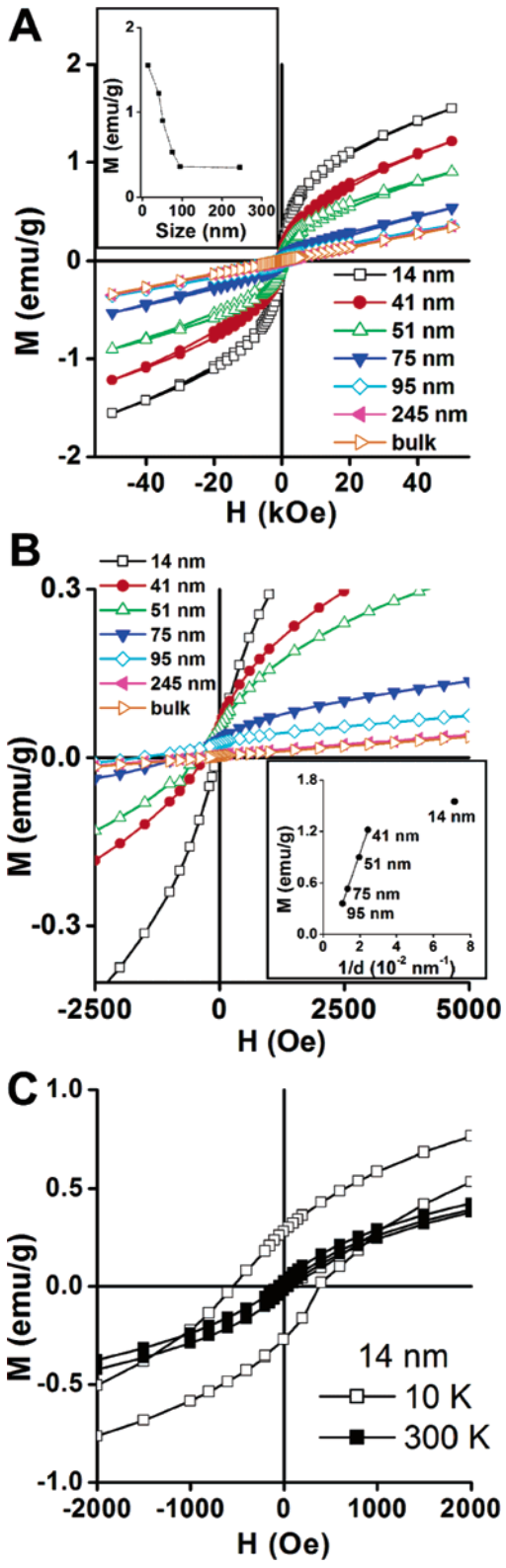

Figure 2. (A) Hysteresis loops at 300 K for $BiFeO_3$ nanoparticles with indicated sizes. The inset shows the magnetization behavior of as-prepared $BiFeO_3$ nanoparticles at 50 kOe as a function of size (diameter, d). (B) Expanded plots of magnetization of as-synthesized $BiFeO_3$ nanoparticles with the return branches of the hysteresis loops omitted for clarity. The inset shows the corresponding magnetization values at 50 kOe as a function of $1/d$. (C) Corresponding magnetization data for the smallest nanoparticle prepared in this study (14 nm) at 10 and 300 K, respectively, are also presented.

Table 1. Derived Room-Temperature Magnetic Parameters[a]

size (d, nm)	$1/d$ (nm^{-1})	M_S at 50 kOe (emu/g)	M_S at 50 kOe (μ_B/Fe)	H_C (Oe)	H_{ex} (Oe)	M_r/M_S
14	0.071	1.55	0.093	58	2.5	0.02
41	0.025	1.22	0.073	305	5	0.05
51	0.020	0.90	0.054	425	25	0.06
75	0.013	0.53	0.032	775	25	0.06
95	0.011	0.36	0.022	1550	50	0.07
245	0.004	0.35	0.021			
bulk		0.34	0.020			

[a] Size (d) represents the diameter of as-prepared $BiFeO_3$ nanoparticles. M_S is the magnetization observed at $H = 50$ kOe. The magnetic moments are defined in units of emu/g as well as in Bohr magnetons per Fe atom (μ_B/Fe). H_C and H_{ex} represent derived coercivities and exchange bias parameters, respectively, while M_r stands for remnant magnetization.

sated spins at the surface. For single-domain antiferromagnetic particles, the magnetization is expected to scale as $\sim 1/d$ (where d is the diameter of the particle), that is, as the surface to volume ratio.[26]

A plot of the magnetization, measured at the maximum applied field of $H_{appl} = 50$ kOe as a function of $1/d$, is presented in the inset to Figure 2B. For particles ranging in diameter from 95 to 41 nm, a linear dependence is observed, indicating that the simple Néel model is applicable.[27] Initially, the ferromagnetic moments on the surface were considered to be oriented along the antiferromagnetic axis of the particle core. It is now believed that the actual microscopic moment arrangement is such that the ferromagnetic surface spins are actually orthogonal to the antiferromagnetic axis of the core.[28] The smallest of the particles measured, i.e., the 14 nm diameter particle, deviates considerably from the expected behavior, indicating that at this particle size range, the particle can no longer be modeled by the superposition of an antiferromagnetic core and a ferromagnetic surface. Rather, as the lattice size diminishes to extremely small particle dimensions, surface strain[29] introduces coordination distortion and lattice disorder that permeate throughout the entire particle, as opposed to being confined only at the surface, with the net result that different frustrated spin structures are produced. In addition, as the particle's magnetization increases, interparticle interactions within the nanoparticle assemblies become stronger, producing a spin-disordered system, as discussed later.

The maximum magnetization, M_S, obtained corresponds to $M_S \sim 1.55$ emu/g for the 14 nm particles. Furthermore, a linear extrapolation of our experimental magnetization data from 75 to 14 nm $BiFeO_3$ nanoparticle samples suggests that the highest magnetization achievable for substrate-free bismuth ferrite nanoparticles can attain values of up to about 1.82 emu/g (0.11 μ_B/Fe). To put this value in context, magnetization values of $0.06-1\ \mu_B$/Fe for epitaxially grown $BiFeO_3$ thin films have been previously reported, although are not considered to be fully determinate.[17,18] By contrast, the magnetization values reported for our as-prepared $BiFeO_3$ nanoparticles represent an attainable magnetization that can be ascribed essentially to size effects alone, without the potentially distracting issues either of epitaxial strain (characteristic of thin films) or of oxygen vacancy defects. We

note that this magnetization attainable from exploiting the sheer size effect of these nanoparticles is relatively small for general applicability in memory devices, although the outlook for specific applications at room temperature, involving spintronics and spin valves, remains highly promising with these nanoscale materials.[30]

The modeling of the magnetization of our particles according to Néel is further supported by the observation of shifted hysteresis loops (Figure 2C), which can be interpreted by the presence of exchange coupling between the ferromagnetic surfaces and the antiferromagnetic cores. Derived coercivities, H_C, and exchange fields, H_{ex}, are given in Table 1. These recorded values, however, most definitely also reflect exchange and dipolar interparticle interactions in addition to interfacial cross grain-boundary interactions due to the high packing volume fraction in our system of particles.[31] As expected, evidence for strong interparticle interactions is provided for by the shape of our hysteresis loops, which exhibit very small remnant magnetization, M_r, for all particles studied and a lack of saturation. Monte Carlo calculations[31] of hysteresis loops of interacting single-domain magnetic particle arrays as a function of particle concentration indicate that the hysteresis loops become progressively tilted toward the x-axis with drastically decreasing M_r/M_S ratios with increasing particle concentration, manifested in this case by an increase in interparticle interactions.

The presence of interparticle interactions can also be gleaned from temperature-dependent magnetization studies presented in Figure 3, as evidenced by the relative insensitivity of particle size with respect to the temperature of maximum magnetization observed. Specifically, magnetization measurements as a function of temperature at an applied field strength of 200 Oe, after zero-field cooling (ZFC) and also with field cooling (FC), were studied (Figure 3). We note that the apparent sharp cusps observed in the magnetization curves at 50 K are reproducible for bismuth ferrite samples with particle dimensions over 95 nm (e.g., 245 nm and bulk), as shown in Figure 3B. For $BiFeO_3$ nanoparticles possessing diameters of $\leq$95 nm, associated data curves exhibit a broad magnetization maximum around $T_{max} = 85$ K, more precisely ranging only from 75 to 95 K. If the observed T_{max} had represented a blocking temperature[32] associated with superparamagnetic relaxation processes of isolated magnetic nanoparticles, one would have expected a much greater dependence of T_{max} on particle size.[33] However, this is not the case. Another feature of the magnetization curves consistent with the presence of interparticle interactions is the more or less linear decrease of the magnetization above T_{max}, whereas for isolated superparamagnetic particles,[34] a $1/T$ dependence would have been expected.[35] Thus, T_{max} represents a spin-glass-like freezing temperature due to the high packing volume fraction as well as a complex interplay between finite size effects,[22,23] interparticle interactions, and a random distribution of anisotropy axes in our nanoparticle assembly.[36]

The electronic and magnetic properties of bismuth ferrite nanoparticles were also systematically investigated by Mössbauer spectroscopy. Mössbauer spectra of $BiFeO_3$ nanoparticles, with typical diameters of 14, 51, and 95 nm, annealed respectively at 400, 500, and 600 °C, are shown in Figure 4, together with corresponding spectra of bulk $BiFeO_3$. As seen in Figure 4a and b, at room temperature, a superposition of quadrupolar (doublet) and magnetic (sixplet) absorption spectra is observed. The spectra become progressively more magnetic with increasing annealing temperature. The collapsed quadrupolar spectra are associated with the subset of smallest particles within the size distribution synthesized within a given sample. Agglomeration leading to the formation of larger particles takes place upon high-temperature annealing, approaching behavior similar to that of bulk material when the average particle size in the distribution measures ~95 nm and above. This tendency to a greater preponderance of larger particles with increasing annealing temperature was also observed in our SEM data.

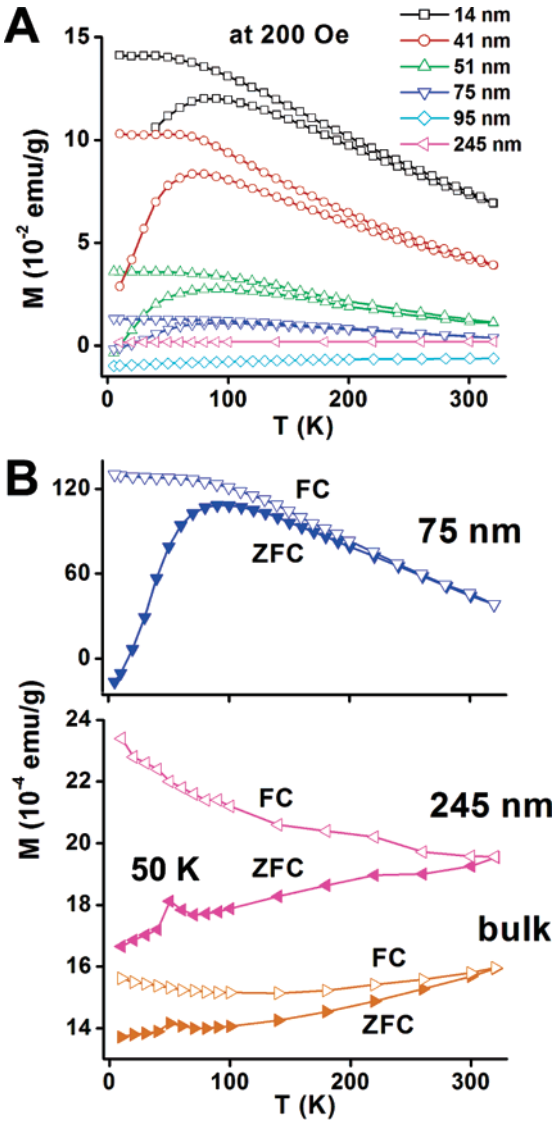

Figure 3. (A) Temperature dependence of the magnetization for $BiFeO_3$ nanoparticles of varying sizes, showing zero field cooling (ZFC) and field cooling (FC) curves, with an applied magnetic field set at 200 Oe. (B) Expanded plots of ZFC and FC curves for $BiFeO_3$ nanoparticles with diameters of 75 and 245 nm, as well as for the bulk, respectively. A sharp cusp is observed for the 245 nm $BiFeO_3$ sample as well as for the bulk and may result from domain wall pinning effects as a result of local structural distortions.[49]

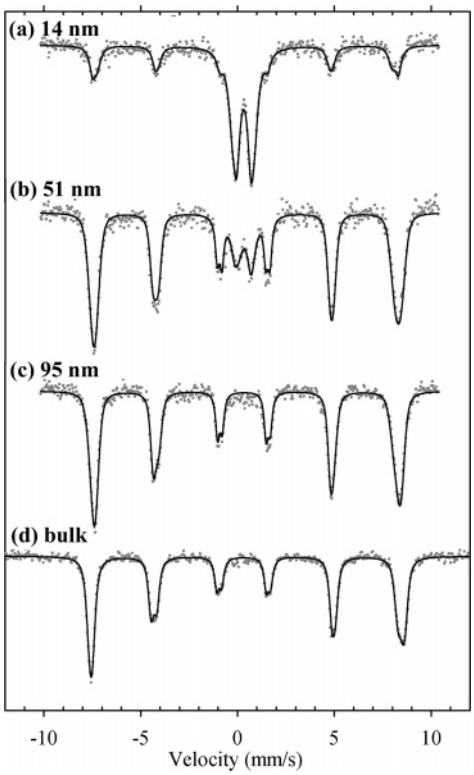

Figure 4. Room-temperature Mössbauer spectra of bulk and as-prepared $BiFeO_3$ nanoparticles, annealed at different temperatures: (a) 14 nm (400 °C), (b) 51 nm (500 °C), (c) 95 nm (600 °C) diameter, and (d) bulk $BiFeO_3$. The solid line is a least-squares fit of the experimental data to theoretical spectra, assuming a superposition of inequivalent iron sites with Lorentzian absorption lines. Derived Mössbauer parameters are tabulated in Table S1 (Supporting Information).

The magnetic spectral signature corresponds to high-spin ferric ions in the $BiFeO_3$ crystal lattice. The characteristic asymmetric, magnetic spectra of the bulk have been previously reported and have been reproduced by our bulk material (Figure 4d).[37] The observed asymmetry has been attributed to the presence of Fe^{3+} in two different crystallographic environments that differ primarily in the size of the electric field gradient.[37] Least-square fits of our experimental data to theoretical spectra give values for the isomer shift (δ), quadrupole splitting (ΔE_Q), and magnetic hyperfine field (H_{hf}) consistent with the presence of high-spin ferric ions (Table S1, Supporting Information).

Above its Néel temperature ($T_N \sim 643$ K), $BiFeO_3$ has been reported to exhibit a single doublet with a quadrupole splitting of about $\Delta E_Q = 0.44$ mm/s, indicating a slightly distorted octahedral symmetry at the Fe^{3+} site.[37] This is consistent with the crystal lattice of $BiFeO_3$, which is known to be a rhombohedrally distorted perovskite structure and in which the Bi^{3+} and Fe^{3+} cations are displaced from their centrosymmetric positions along the (111) axis. Below T_N, the magnetic interaction dominates, with the quadrupolar interaction contributing a small perturbation to the observed overall magnetic structure.

Above the spin-glass-like freezing temperature, thermal activation and fluctuations can induce fast reversals of the particle's magnetic moment, leading to the observation of zero average internal magnetic field.[24,38] The smallest particles in the distribution, with a blocking temperature for the characteristic measuring time of Mössbauer spectroscopy $T_{B(Möss)} < 300$ K, will experience such sufficiently fast spin reversals at room temperature that a collapse of their magnetic spectra to quadrupolar spectra is expected. These particular systems are composed primarily of two inequivalent subsites that differ in the degree of site coordination distortion, as reflected by the values of the quadrupole splitting ($\delta_1 = 0.32$ mm/s, $\delta_2 = 0.31$ mm/s, $\Delta E_{Q1} = 0.71$ mm/s, $\Delta E_{Q2} = 1.09$ mm/s for the 400 °C annealed sample with average particle size of 14 nm, Table S1). We note that the observed quadrupole splittings of the superantiferromagnetic state are larger than that of the paramagnetic state, above the Néel temperature. It is reasonable to postulate that surface imperfections and surface strain anisotropies[29] in the smaller particles induce distortion and site inequivalence on the crystallographic structure, resulting in an increase in the value of ΔE_Q due to magnetostrictive effects.[39] This observation is in accordance with the known multiferroic behavior of this system and the strong coupling between dielectric and magnetic properties.[40] For larger particles, two inequivalent magnetic subsites are observed with slightly different values of magnetic hyperfine fields ($H_{hf1} = 484$ kOe and $H_{hf2} = 489$ kOe for the 95 nm, 600 °C annealed sample; Table S1). These values are consistent with previously reported values for bulk $BiFeO_3$ at 80 K by $^{57}Fe-$Mössbauer and $^{57}Fe-$NMR spectroscopies.[37,41]

As discussed earlier, oxygen deficiency in the $BiFeO_3$ structure is known to produce leakage problems, compromising this promising material from device applications. Mössbauer spectroscopy is uniquely suited for the detection of oxygen deficiency due to the fact that it results in the reduction of $Fe^{3+} \rightarrow Fe^{2+}$ at the location of the oxygen vacancy. We have carefully examined our spectroscopic data for the presence of Fe^{2+}. No such signal was detected for any of our annealed samples with particles possessing a diameter, $d \geq 14$ nm. We also recorded the Mössbauer spectra of a sample that was not annealed, but rather had been only preheated at 300 °C (Figure S5, Supporting Information). Because of the small size, ≤14 nm, of the particles, the room-temperature spectra evince a superparamagnetic signature, while at 4.2 K, the full magnetic spectrum is recovered (Figure S5). This is the only spectrum exhibiting a very weak Fe^{2+} signature, ≤2% effect, contributing no more than 0.01 μ_B/Fe to the observed magnetic signal (Figure S5). Hence, the large increase in magnetization observed with decreasing particle size cannot be explained away by the presence of Fe^{2+}, that is, the presence of oxygen defects. Instead, the increase in magnetization is due primarily to the fact that, as the particle size diminishes and the surface-to-volume ratio increases, the contribution of surface spins to the total magnetic moment of the particle increases.[42] It is well-established that surface anisotropies dominate magnetic behavior in small particles. Thus, we believe that the increase of magnetization in our nanoscale bismuth ferrite nanoparticles is due primarily to the contribution of uncompensated spins at the surface, strain anisotro-

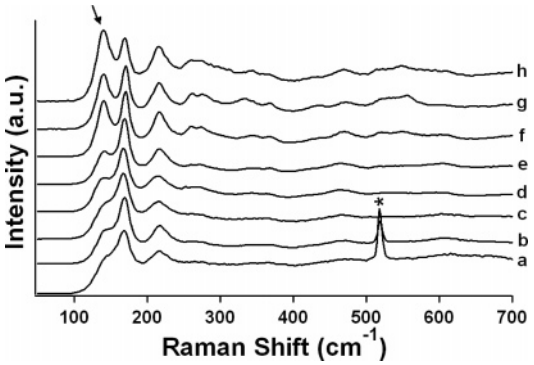

Figure 5. Raman spectra of as-prepared $BiFeO_3$ nanoparticles with typical dimensions of (a) 14 nm, (b) 41 nm, (c) 51 nm, (d) 75 nm, (e) 95 nm, (f) 245 nm, and (g) 342 nm, respectively, as well as of the bulk (h). The Si substrate peaks have been indicated by an asterisk (a and b). The arrow is referring to the peak at 136 cm^{-1}, corresponding to the first normal A_1 mode of bulk $BiFeO_3$.

pies, and noncollinear magnetic ordering, leading to frustrated spin systems in addition to an increased suppression of the material's intrinsic spiral spin structure below a certain particle size, as previously discussed.[43]

To look for evidence of any coupling between the magnetic and electric properties in our nanoscale system as well as to corroborate our SQUID and Mössbauer data, we also completed a Raman study of randomly oriented, as-prepared $BiFeO_3$ nanoparticles, shown in Figure 5. The peak at 136 cm^{-1} (denoted by an arrow, Figure 5) can be assigned to the first normal A_1 mode for the rhombohedral $BiFeO_3$ system.[44] The decrease in peak intensity of this normal A_1 mode with decreasing particle size is indicative of the suppression in the contribution of the Bi-O1 vibrational mode, which can most likely be attributed to enhanced coupling of magnetic, ferroelectric, and/or structural order parameters due to size confinement considerations and accompanying lattice distortions in as-prepared $BiFeO_3$ nanoparticles. The decrease in the intensity of the 136 cm^{-1} peak, observed for $BiFeO_3$ nanoparticles with size ranges up to 95 nm (Figure 5a−e), coincides with the appearance of an appreciable spontaneous magnetization and hysteretic behavior in corresponding SQUID measurements (Figure 2). By contrast, the lack of an appreciable hysteresis in SQUID data was correlated with an increased intensity of the 136 cm^{-1} Raman peak for $BiFeO_3$ samples larger than 95 nm (Figure 5f and g). We also note by means of comparison that the Raman spectrum of bulk $BiFeO_3$ samples, shown in Figure 5h, is in good agreement with that of previously reported data.[45]

In summary, this is the first reported study of the synthesis and characterization of pure-phase, substrate-free, and relatively strain-free (as compared with epitaxially grown films)[46] single-crystalline $BiFeO_3$ nanoparticle specimens. Our nanoparticles exhibit size-dependent magnetic behavior wherein the particles are analogous to incomplete magnetic supercells that retain a net magnetic moment. The critical observations relevant to potential applications are (a) increased magnetization values at the nanoscale due to size-confinement effects at room temperature and (b) the presence of insignificant amounts of Fe^{2+}, indicating the absence or great suppression of defects associated with oxygen deficiency. Oxygen vacancies that contribute to leakage problems in ceramic preparations of $BiFeO_3$ are primarily responsible for hindering potential device applications.[47,48] Suppression of oxygen vacancies is known to increase the resistivity and multiferroic behavior of these systems. Thus, samples derived from our nanoscale systems should possess high resistivity and enhanced multiferroic properties with promising potential. The observation of hysteresis at room temperature is especially auspicious and could be further enhanced by rationally tailored shape anisotropy.

Acknowledgment. The Mössbauer investigations at Villanova University were supported by NSF under contract no. DMR-0604049. S.S.W. acknowledges the U.S. Department of Energy under contract no. DE-AC02-98CH10886 for facility usage and personnel support and the NSF (CAREER award DMR-0348239) for PI support and supplies. S.S.W. is an Alfred P. Sloan Research Fellow (2006−2008). Dr. James Quinn (Stony Brook) is acknowledged for his help with SEM and TEM. We also thank Dr. Yuanbing Mao (Stony Brook) and Prof. Jianyu Huang (Boston College) for their assistance with HRTEM results. Dr. Tirandai Hemraj-Benny (Stony Brook) and Dr. Zhorro Nikolov (Drexel) are recognized for their collection of Raman spectroscopy data. We also acknowledge Drs. Kyungha Kang (Brookhaven National Laboratory), K. Trohidou (NCSR Demokritos), and C. Binns (University of Leicester) for valuable discussions.

Supporting Information Available: Materials and Methods, figures, and table. This material is available free of charge via the Internet at http://pubs.acs.org.

References

(1) Schmid, H. *Ferroelectrics* **1994**, *162*, 317−338.
(2) Eerenstein, W.; Mathur, N. D.; Scott, J. F. *Nature* **2006**, *442*, 759−765.
(3) Smolenskii, G. A.; Chupis, I. E. *Sov. Phys. Usp.* **1982**, *25*, 475−493.
(4) Fiebig, M. *J. Phys. D: Appl. Phys.* **2005**, *38*, R123−R152.
(5) Fiebig, M.; Lottermoser, T.; Fröhlich, D.; Goltsev, A. V.; Pisarev, R. V. *Nature* **2002**, *419*, 818−820.
(6) Hur, N.; Park, S.; Sharma, P. A.; Ahn, J. S.; Guha, S.; Cheong, S.-W. *Nature* **2004**, *429*, 392−395.
(7) Wang, J.; Neaton, J. B.; Zheng, H.; Nagarajan, V.; Ogale, S. B.; Liu, B.; Viehland, D.; Vaithyanathan, V.; Schlom, D. G.; Waghmare, U. V.; Spaldin, N. A.; Rabe, K. M.; Wuttig, M.; Ramesh, R. *Science* **2003**, *299*, 1719−1722.
(8) Ederer, C.; Spaldin, N. A. *Phys. Rev. B* **2005**, *71*, 224103−224109.
(9) Sosnowska, I.; Peterlin-Neumaier, T.; Steichele, E. *J. Phys. C: Solid State Phys.* **1982**, *15*, 4835−4846.
(10) Park, T.-J.; Mao, Y.; Wong, S. S. *Chem. Commun.* **2004**, 2708−2709.
(11) Ghosh, S.; Dasgupta, S.; Sen, A.; Maiti, H. S. *J. Am. Ceram. Soc.* **2005**, *88*, 1349−1352.
(12) Yun, K. Y.; Noda, M.; Okuyama, M.; Saeki, H.; Tabata, H.; Saito, K. *J. Appl. Phys.* **2004**, *96*, 3399−3403.
(13) Qi, X.; Dho, J.; Blamire, M.; Jia, Q.; Lee, J. S.; Foltyn, S.; MacManus-Driscoll, J. L. *J. Magn. Magn. Mater.* **2004**, *283*, 415−421.
(14) Singh, S. K.; Kim, Y. K.; Funakubo, H.; Ishiwara, H. *Appl. Phys. Lett.* **2006**, *88*, 162904/1−162904/3.
(15) Lee, Y.-H.; Wu, J.-M.; Chen, Y.-C.; Lu, Y.-H.; Lin, H.-N. *Electrochem. Solid State Lett.* **2005**, *8*, F43−F46.

(16) Wang, Y.; Jiang, Q.-H.; He, H.-C.; Nan, C.-W. *Appl. Phys. Lett.* **2006**, *88*, 142503/1−142503/3.
(17) Eerenstein, W.; Morrison, F. D.; Dho, J.; Blamire, M. G.; Scott, J. F.; Mathur, N. D. *Science* **2005**, *307*, 1203a.
(18) Wang, J.; Scholl, A.; Zheng, H.; Ogale, S. B.; Viehland, D.; Schlom, D. G.; Spaldin, N. A.; Rabe, K. M.; Wuttig, M.; Mohaddes, L.; Neaton, J.; Waghmare, U.; Zhao, T.; Ramesh, R. *Science* **2005**, *307*, 1203b.
(19) Neaton, J. B.; Ederer, C.; Waghmare, U. V.; Spaldin, N. A.; Rabe, K. M. *Phys. Rev. B* **2005**, *71*, 014113−014118.
(20) Ederer, C.; Spaldin, N. A. *Phys. Rev. B* **2005**, *71*, R060401−R060404.
(21) Tokura, Y. *Science* **2006**, *312*, 1481−1482.
(22) Sosnowska, I.; Schäfer, W.; Kockelmann, W.; Andersen, K. H.; Troyanchuk, I. O. *Appl. Phys. A* **2002**, *74*, S1040−S1042.
(23) Néel, L. *Compt. Rend.* **1961**, *252*, 4075−4080.
(24) Néel, L. *Compt. Rend.* **1961**, *252*, 9−12.
(25) Néel, L. *Compt. Rend.* **1961**, *253*, 203−208.
(26) Richardson, J. T.; Yiagas, D. I.; Turk, B.; Forster, K.; Twigg, M. V. *J. Appl. Phys.* **1991**, *70*, 6977−6982.
(27) Néel, L. In *Low Temperature Physics*; DeWitt, C., Dreyfus, B., DeGennes, P. G., Eds.; Gordon and Beach: London, 1962; p 411.
(28) O'Handley, R. C. *Modern Magnetic Materials, Principles, and Applications*; John Wiley & Sons: New York, 1999.
(29) Papaefthymiou, G. C. *J. Magn. Magn. Mater.* **2004**, *272*, E1227−E1229.
(30) Dho, J.; Qi, X.; Kim, H.; MacManus-Driscoll, J. L.; Blamire, M. G. *Adv. Mater.* **2006**, *18*, 1445−1448.
(31) Lamba, S.; Annapoorni, S. *Eur. Phys. J. B* **2004**, *39*, 19−25.
(32) Néel, L. *Ann. Geophys.* **1949**, *5*, 99−136.
(33) Mamiya, H.; Nakatani, I.; Furubayashi, T. *Phys. Rev. Lett.* **1998**, *80*, 177−180.
(34) Krechrakos, D.; Trohidou, K. N. *Phys. Rev. B* **1998**, *58*, 12169−12177.
(35) Binns, C.; Maher, M. J.; Pankhurst, Q. A.; Kechrakos, D.; Trohidou, K. N. *Phys. Rev. B* **2002**, *66*, 184413/1−184413/11.
(36) Labarta, A.; Battle, X.; Iglesias, O. In *Surface Effects in Magnetic Nanoparticles*; Fiorani, D., Ed.; Springer: Berlin, 2005.
(37) Blaauw, C.; van der Woude, F. *J. Phys. C; Solid State Phys.* **1973**, *6*, 1422−1431.
(38) Brown, W. F., Jr. *J. Appl. Phys.* **1968**, *39*, 993−994.
(39) del Moral, A. *Magnetostriction: Principles and Applications*; Institute of Physics Publications: Bristol, U.K. 2004.
(40) Salje, E. K. H. *Phase Transitions in Ferroelectric and Co-elastic Crystals*; Cambridge University Press: Cambridge, 1990.
(41) Zalessky, A. V.; Frolov, A. A.; Khimich, T. A.; Bush, A. A.; Pokatilov, V. S.; Zvezdin, A. K. *Europhys. Lett.* **2000**, *50*, 547−551.
(42) Park, T.-J.; Papaefthymiou, G. C.; Moodenbaugh, A. R.; Mao, Y.; Wong, S. S. *J. Mater. Chem.* **2005**, *15*, 2099−2105.
(43) Coey, J. M. D. *Phys. Rev. Lett.* **1971**, *27*, 1140−1142.
(44) Singh, M. K.; Ryu, S.; Jang, H. M. *Phys. Rev. B* **2005**, *72*, 132101−132104.
(45) Nadifi, H.; Ouali, A.; Grigorescu, C.; Faqir, H.; Monnereau, O.; Tortet, L.; Vacquier, G.; Boulesteix, C. *Supercond. Sci. Technol.* **2000**, *13*, 1174−1179.
(46) Jiang, Q.; Qiu, J. H. *J. Appl. Phys.* **2006**, *99*, 103901/1−103901/6.
(47) Pradhan, A. K.; Zhang, K.; Hunter, D.; Dadson, J. B.; Loiutts, G. B.; Bhattacharya, P.; Katiyar, D. J.; Zhang, J.; Sellmyer, D. J.; Roy, U. N.; Cui, Y.; Burger, A. *J. Appl. Phys.* **2005**, *97*, 093903−093906.
(48) Wang, Y. P.; Zhou, L.; Zhang, M. F.; Chen, X. F.; Liu, J.-M.; Liu, Z. G. *Appl. Phys. Lett.* **2004**, *84*, 1731−1733.
(49) Sankar, C. R.; Joy, P. A. *Phys. Rev. B* **2005**, *72*, 024405/1−024405/10.

NL063039W